공학 석사 학위 논문

Vibration and Buckling Analysis of Multifunctional Antenna Structures with Thermoelastic Characteristics

열 효과를 고려한 다기능 내장 안테나 구조물의 진동과 좌굴 해석

2017년 2월

서울대학교 대학원

기계항공공학부

강 석 현

열 효과를 고려한 다기능 내장 안테나 구조물의 진동과 좌굴 해석

Vibration and Buckling Analysis of Multifunctional Antenna Structures with Thermoelastic Characteristics

지도교수 김 지 환

이 논문을 공학석사 학위논문으로 제출함

2017 년 2 월

서울대학교 대학원
기계항공공학부
강 석 현

강석현의 공학석사 학위논문을 인준함

2017 년 2 월

위 원 장 김 용 협

부위원장 김 지 환

위 원 신 상 준

Abstract

The performance of multifunctional antenna structure contained inside of the aircraft structure is analyzed under the influence of vibration caused by airflow and a thermal environment. The model is a multi-layer sandwich structure composed of carbon/epoxy, glass/epoxy and a dielectric polymer which is assumed to be an antenna. The First-order Shear Deformation Theory (FSDT) is used with a modified shear correction factor. In order to account for a geometrical nonlinearity, the governing equations are based on the von-Karman displacement-strain relationship with the principle of virtual work. Additionally, using the first-order piston theory, the effect of aerodynamic pressure is represented in the equation. The Newton-Rhapson iteration and the Newmark method is used to solve the nonlinear equation and the time analysis, respectively. Also, neutral surface and shear correction factor concepts are studied for unsymmetric models. The thermal environment is generally considered with one-dimensional heat conduction equations. To check the validity of the results, it is compared to the numerical data of vibration and buckling from previous studies. Post-buckling and flutter analysis is performed with simply-supported and clamped boundary conditions.

Keywords: Multifunctional antenna structure, Buckling, Vibration, Flutter, Heat conduction.

Student Number: 2015-20763

Contents

List of Tables and Figures

Tables

Figures

List of Nomenclature

k	Thermal conductivity
u_0	Mid-plane displacement in x-direction
v_0	Mid-plane displacement in y-direction
w_0	Mid-plane displacement in z-direction
ϕ_x	Rotations of the transverse normal in the xz planes
ϕ_y	Rotations of the transverse normal in the yz planes
z_n	Distance between middle and neutral plane
$\boldsymbol{\varepsilon_{\alpha\beta}}$	In-plane strain vector
$\boldsymbol{\varepsilon^0_{\alpha\beta}}$	In-plane strain vector at the mid-plane
$\boldsymbol{\kappa_{\alpha\beta}}$	Curvature strain vector
$\boldsymbol{\gamma_{\alpha 3}}$	Transverse shear strain vector
$\boldsymbol{\sigma}$	In-plane stress vector
$\boldsymbol{\alpha}$	Thermal expansion coefficients vector
ΔT	Temperature variation
$\overline{Q}_{ij}$	Transformed stiffness coefficients matrix
$\boldsymbol{N_b}$	Force resultant vector
$\boldsymbol{M_b}$	Moment resultant vector
$[\mathrm{A}]$	Extensional stiffness matrix
$[\mathrm{B}]$	Bending-extension coupling stiffness matrix
$[\mathrm{D}]$	Bending-twist coupling stiffness matrix
$[\mathrm{S}]$	Shear stiffness matrix
$\boldsymbol{N_{\Delta T}}$	Thermal force vector
$\boldsymbol{M_{\Delta T}}$	Thermal moment vector
δW_{int}	Internal virtual work
δW_{ext}	External virtual work
$\boldsymbol{d}$	Displacement vector
$\boldsymbol{P_{\Delta T}}$	Thermal load vector
$\boldsymbol{K}$	Linear elastic stiffness matrix
$\boldsymbol{K_{\Delta T}}$	Thermal geometric stiffness matrix

$\boldsymbol{KN}_1$	First order non-linear stiffness matrix
$\boldsymbol{KN}_2$	Second order non-linear stiffness matrix
$\boldsymbol{M}$	Mass matrix
$\boldsymbol{f}$	External force vector
p_a	Aerodynamic pressure
V_∞	Air flow speed
M_∞	Mach number
ρ_a	Air density
λ	Non-dimensional aerodynamic pressure
ω_0	Convenient reference frequency
β	Aerodynamic pressure parameter
D_m	Bending rigidity
a	Length of the skin
h	Thickness of the skin
μ	Air-mass ratio
g_a	Non-dimensional aerodynamic damping parameter
$\boldsymbol{A}_f$	Aerodynamic influence matrix
$\boldsymbol{A}_d$	Aerodynamic damping matrix
T_{cr}	Critical temperature
κ_p	Shear correction factor
ω	Natural frequency
$\boldsymbol{\Phi}$	Generalized displacement vectors
$\boldsymbol{\Phi}_0$	Time independent vector

1. Introduction

A multifunctional antenna structure is designed to provide two different functions in the field of military aircraft [1]. One such structure is the Conformable Load-bearing Antenna Structure (CLAS) with antennas in load-bearing aircraft skins. The concept of CLAS is to replace separate aircraft structure and antennas. The benefits of the CLAS structure are reducing drag and enhancing structural efficiency [2]. Furthermore, reducing the outside antennas will decrease the radar cross-section (RCS) of an aircraft, thus increasing its stealth function. Such advantageous characteristics have served to provide momentum to this field of research. However, there are some limitations such as design complexity and antenna performance. For example, the structure of flight vehicles are deformed from thermal and aerodynamic loads. The deformation caused by the static and dynamic behaviors may influence the antenna performance and may even lead to structural failure. In this paper, mechanical behaviors, such as vibration, post-buckling, and flutter are presented with consideration of antenna performance.

Many researchers designed CLAS to improve its benefits. Varadan and Varadan [3] studied the concept to use the lower skin of the radome as a substrate on which the radiator can be made using standard photolithography. The Structures Division of the US Air Force's Wright Laboratory is sponsoring the demonstration of CLAS.[4]. In this study, a multifunctional antenna component panel that could withstand loads of 4000 pounds per inch is researched. Callus [2] described the state-of-the-art in CLAS technology through a review of the open-source literature. It focuses

on CLAS study for demonstrators of Very High Frequency (VHF) and X-band communication applications have been successfully designed, analyzed, manufactured and tested. Additionally, You et al. [5] designed a load-bearing outer composite surface that enhanced antenna performance. The results of this study is that antenna efficiency can be improved with structurally effective materials of high electrical loss. On the same note, antenna performance of CLAS have been studied. Bishop [6] researched size reduced ultrawideband (UWB) antenna arrays of CLAS. Additionally, vibration control of CLAS is analyzed to reduce the effects from aero-dynamical loads which cause vibration and deformation of the structure and degrade the antenna performance[7,8]. Loecker et al. [9] studied the way to overcome vibrations of an antenna array using active vibration control by integrating sensors and actuators into the antenna structure.

In order to understand the mechanical behaviors of these structures as antennas and load bearers, the characteristics of the basic model, which is a composite sandwich structure, needs to be analyzed. Pradeep and Ganesan [10] studied the vibration behavior and thermal buckling of multi-layer rectangular sandwich plates considering the temperature-dependent characteristics of the complex shear modulus for a viscoelastic core. Matsunaga [11] analyzed a higher-order shear deformation model for stability behavior and dynamic response of angle-ply laminates composite and sandwich plates under thermal loading. Then, the critical state was obtained by increasing temperature until the natural frequency was reduced to zero. Roh et al. [12] studied these analyses of composite conical shells based on the layerwise theory and von-Karman displacement strain relationships. Also, the structural stability of the shells subjected to the thermal load was also observed. Park et al. [13] investigated that the

composite plate embedded with shape memory alloy fibers were subjected to aerodynamic and thermal loading in the supersonic region.

In recent years, the mechanical behaviors of CLAS were analyzed. Gibson [14] reported a review of recent research on the mechanics of multifunctional composite materials and structures. Many applications of the structures as well as a basic theory and materials are investigated in this article. Jeon et al. [15] investigated buckling characteristics of smart skin structures designed in a composite sandwich structure and a multi-layer micro strip antenna. Lee and Kim [16] analyzed thermal stability characteristics and limit cycle oscillation of smart skin structures for the different sizes and shapes of dielectric portion within an enclosure layer.

However, little research exists for the mechanical behavior of the model in a thermal environment, and is related to uniform temperature condition. In this paper, the heat conduction concept is considered. It is predicted that the stability boundary of the model will change and other characteristics of vibration will be analyzed.

To start learning about the relationship between antenna performance and mechanical behavior, the present work is studied with vibration, post-buckling and flutter analyses of the structure model based on the composite sandwich structure made by a honeycomb core, carbon/epoxy, glass epoxy in a thermal environment. Also, antenna platform of dielectric layer is assumed to consist of phenol [17]. This model is based on the First-order Shear Deformation Theory (FSDT) and von-Karman relations for large deformation. Additionally, the neutral surface and the shear correction factor is modified for unsymmetric characteristics. To obtain the validity of the present work, the results are compared with previous data. Also, the first-order piston theory is adopted for modeling aerodynamic loads. The

numerical result shows the effect of the heat conduction concept on the suppression of the thermal deflection and panel flutter.

2. Modeling and Formulations

Fig. 1 shows the model of a multifunctional antenna structure which consisted of five layers with four materials including glass/epoxy, carbon/epoxy, dielectric layer and honeycomb core. Using the increment method of temperature, one-dimensional heat equation and thermal boundary condition is applied for simply-supported plates. Additionally, based on the first-order shear deformation plate theory, the governing equations of the model are taken from the principle of virtual work.

2.1 Heat Conduction

To consider incremental displacement, the temperature rise dT from the reference temperature T_{ref} is followed by small temperature increment ΔT [18]. T_0 and d_0 mean the temperature and displacement of initial state. Based on this temperature rise, the strain-stress relationships are derived.
Additionally, the steady-state heat conduction equation are taken as thermal boundary condition. Temperature is dependent on the equation only one-dimensional change which is z direction.

$$\frac{d}{dz}\left[k(z)\frac{dT}{dz} \right] = 0 \tag{1}$$

where $k(z)$ is the coefficient of the model and dependent on z. In here, the thermal conductivity in the vertical direction is not related to fiber angle[19,20]. And then, the temperature of each layer is decided from this

coefficient and equation. Also, the boundary conditions are expressed as following:

$$T_1 = T_b = T_{ref}\,, \quad T_6 = T_u \tag{2}$$

$$T_i\big|_{z=zi} = T_{i+1}\big|_{z=zi}\,, \quad k_i \left.\frac{dT_i}{dz}\right|_{z=zi} = k_{i+1} \left.\frac{dT_{i+1}}{dz}\right|_{z=zi} \quad (i = 2,3,4,5) \tag{3}$$

where the subscript b and u are the meaning of bottom and top face, respectively. At each inter face, the heat conductivity and temperature should be equal as boundary conditions.

2.2 Constitutive Equation

A present model is based on the first-order shear deformation theory, the displace and strain field are presented as

$$\begin{aligned} u_\alpha(x,y,z) &= u^\circ_\alpha(x,y) + (z - z_n)\phi_\alpha(x,y) \quad (\alpha = 1,2) \\ w(x,y,z) &= w^\circ(x,y) \end{aligned} \tag{4}$$

where u°_α and w° are the mid-plane displacement in the $x(\alpha = 1), y(\alpha = 2)$ and z directions, respectively. The rotation of the transverse normal in the xz and yz planes are ϕ_α. Additionally, z_n is the distance between neutral surface and middle surface as following[21] :

$$z_n = \frac{\int_{-h/2}^{+h/2} \bar{Q}_{xx}(z) z dz}{\int_{h/2}^{+h/2} \bar{Q}_{xx}(z)} = \frac{\frac{1}{2}\sum_{k=1}^{n} (\bar{Q}_{xx})_k (z_k{}^2 - z_{k-1}{}^2)}{\sum_{k=1}^{n} (\bar{Q}_{xx})_k (z_k - z_{k-1})} \quad (5)$$

where $\bar{Q}_{xx}$ is the value of transferring to x-direction from $E_{11}/(1-\nu_{12}\nu_{21})$. In post-buckling analysis, neutral surface influence more than expected due to the nonlinear term.

Additionally, the von-Karman strain-displacement relations are [22]

$$\varepsilon_{\alpha\beta} = \frac{1}{2}\left(u_{a,\beta} + u_{\beta,\alpha} + w_{,\alpha} w_{,\beta}\right) \ (\alpha, \beta = 1, 2) \ (2) \quad (6)$$

where $\varepsilon_{\alpha\beta}$ is the in-plane strains. Substituting Eq. (4) into Eq. (5),

$$\varepsilon_{\alpha\beta} = \varepsilon^0{}_{\alpha\beta} + (z - z_n)\ \kappa_{\alpha\beta} \quad (7)$$

where $\varepsilon^0{}_{\alpha\beta}$ and $\kappa_{\alpha\beta}$ are in-plane strain vector at the neutral surface and the curvature strain vectors, respectively. Additionally, the transverse shear strain vector is derived as

$$\gamma_{\alpha 3} = \left\{\phi_\alpha + w_{,\alpha}\right\} \quad (8)$$

Therefore, the stress-strain relation is expressed as

$$\boldsymbol{\sigma} = [C](\boldsymbol{\varepsilon} - \boldsymbol{\alpha}\Delta T) \tag{9}$$

To analyze the laminated plate, the force and shear resultant vectors are $\boldsymbol{N_b}$ and $\boldsymbol{M_b}$.

$$\begin{Bmatrix} \boldsymbol{N_b} \\ \boldsymbol{M_b} \end{Bmatrix} = \begin{bmatrix} \mathrm{A} & \mathrm{B} \\ \mathrm{B} & \mathrm{D} \end{bmatrix} \begin{Bmatrix} \boldsymbol{\varepsilon}^0 \\ \boldsymbol{\kappa} \end{Bmatrix} - \begin{Bmatrix} \boldsymbol{N}_{\Delta \boldsymbol{T}} \\ \boldsymbol{M}_{\Delta \boldsymbol{T}} \end{Bmatrix} \quad , \quad \mathbf{Q} = [\mathrm{S}]\boldsymbol{\gamma} \tag{10}$$

$$(\mathrm{A,B,D}) = \sum_{k=1}^{n} \int_{z_{k-1}}^{z_k} (\bar{Q}_{ij})_k (1, z_N, {z_N}^2) dz \ (i, \mathrm{j} = 1, 2, 6) \tag{11}$$

$$[\mathrm{S}] = \sum_{k=1}^{n} k_p \int_{z_{k-1}}^{z_k} (\bar{Q}_{ij})_k dz \ (i, \mathrm{j} = 4, 5) \tag{12}$$

where k_p is shear correction factor. The thermal force $\boldsymbol{N}_{\Delta \boldsymbol{T}}$ and $\boldsymbol{M}_{\Delta \boldsymbol{T}}$ are

$$(\boldsymbol{N}_{\Delta \boldsymbol{T}}, \boldsymbol{M}_{\Delta \boldsymbol{T}}) = \sum_{k=1}^{n} \int_{z_{k-1}}^{z_k} \left[\bar{Q}_{ij}\right]_k \boldsymbol{\alpha}_k (1, z_N) \Delta T dz \quad (i, j = 1, 2, 3) \tag{13}$$

In addition, $\boldsymbol{\alpha}$ are defined as $\boldsymbol{\alpha} = [\boldsymbol{\alpha}_x \ \boldsymbol{\alpha}_y \ \boldsymbol{\alpha}_{xy}]^T$

$$\begin{aligned} \alpha_x &= \alpha_1 \cos^2\theta + \alpha_2 \sin^2\theta \\ \alpha_y &= \alpha_1 \sin^2\theta + \alpha_2 \cos^2\theta \\ \alpha_{xy} &= 2(\alpha_1 - \alpha_2) \sin\theta \cos\theta \end{aligned} \tag{14}$$

where α_1, α_2 are the thermal expansion coefficients, respectively, and θ is the ply angle.

2.3 Governing Equation

Using the principle of virtual work, the governing equation is derived.

$$\delta W = \delta W_{\text{int}} - \delta W_{ext} = 0 \tag{15}$$

where the external virtual work δW_{ext} and internal virtual work δW_{int} are presented as following

$$\begin{aligned} \delta W_{\text{int}} &= \int_{\boldsymbol{A}} \boldsymbol{\delta\varepsilon}^{\boldsymbol{T}} \boldsymbol{N_b} + \boldsymbol{\delta\kappa}^{\boldsymbol{T}} \boldsymbol{M_b} + \boldsymbol{\delta\gamma}^{\boldsymbol{T}} \mathbf{Q} \; dA \\ &= \delta \boldsymbol{d}^{\boldsymbol{T}} [\boldsymbol{K} - \boldsymbol{K}_{\Delta \boldsymbol{T}} + \frac{1}{2} \boldsymbol{K}\boldsymbol{N}_1 + \frac{1}{3} \boldsymbol{K}\boldsymbol{N}_2] \boldsymbol{d} - \delta \boldsymbol{d}^{\boldsymbol{T}} \boldsymbol{P}_{\Delta \boldsymbol{T}} \end{aligned} \tag{16}$$

where $\boldsymbol{d} = \left\{\phi_x, \phi_y, u, v, w\right\}^T$ and $\boldsymbol{\sigma} = \left\{\sigma_{xx}, \sigma_{yy}, \tau_{xy}\right\}$ are displacement and stress vectors, also, $\boldsymbol{K}$, $\boldsymbol{K}_{\Delta \boldsymbol{T}}$, $\boldsymbol{K}\boldsymbol{N}_1$, $\boldsymbol{K}\boldsymbol{N}_2$ and $\boldsymbol{P}_{\Delta \boldsymbol{T}}$ represent the linear elastic stiffness, thermal geometric stiffness, the first-order nonlinear stiffness, the second-order nonlinear stiffness matrices and thermal load vector, respectively. Especially, $\boldsymbol{K}_{\Delta \boldsymbol{T}}$ is derived as

$$\delta W_{\Delta T} = -\int_{\boldsymbol{A}} \boldsymbol{\delta\varepsilon}^{\boldsymbol{T}} \boldsymbol{N}_{\Delta \boldsymbol{T}} \; dA = -\iint_{\boldsymbol{A}} \boldsymbol{N}_{\Delta \boldsymbol{T}x} \; \delta\left(\frac{\partial w}{\partial x}\right) + \boldsymbol{N}_{\Delta \boldsymbol{T}y} \; \delta\left(\frac{\partial w}{\partial y}\right) + \boldsymbol{N}_{\Delta \boldsymbol{T}xy} \; \delta\left(\frac{\partial w}{\partial x}\right)\left(\frac{\partial w}{\partial y}\right) dA$$

$$= \delta \boldsymbol{d}^{\boldsymbol{T}} \boldsymbol{K}_{\Delta \boldsymbol{T}} \boldsymbol{d} \tag{17}$$

The external virtual work are presented as

$$\delta W_{ext} = \int_A [-I_0(\ddot{u}_0 \delta u_0 + \ddot{v}_0 \delta v_0 + \ddot{w}_0 \delta w_0) - I_1(\ddot{u}_0 \delta \phi_x + \ddot{\phi}_x \delta u_0 + \ddot{v}_0 \delta \phi_y + \ddot{\phi}_y \delta v_0) - I_2(\ddot{\phi}_x \delta \phi_x + \ddot{\phi}_y \delta \phi_y) + p_a \delta w] dA$$

$$= \delta \boldsymbol{d}^{\boldsymbol{T}} \boldsymbol{M} \ddot{\boldsymbol{d}} + \delta \boldsymbol{d}^{\boldsymbol{T}} \boldsymbol{f} \tag{18}$$

where $(I_0, I_1, I_2) = \int_{-h/2}^{h/2} \rho(1, z, z^2) dz$ and $\boldsymbol{M}$ is the mass matrix.

A aerodynamic pressure caused by a supersonic air flow is taken into account in the external force. It is assumed by the first-order piston theory for the range of $\sqrt{2} < M_\infty < 5$ [23]. The aerodynamic force are expressed as

$$\begin{aligned} p_a(x, y, t) &= -\frac{\rho_a V_\infty^2}{\sqrt{M_\infty^2 - 1}} \left\{ \frac{\partial w}{\partial x} + \left(\frac{M_\infty^2 - 2}{M_\infty^2 - 1} \right) \frac{1}{V_\infty} \frac{\partial w}{\partial t} \right\} \\ &= -\left(\lambda \frac{D_m}{a^3} \frac{\partial w}{\partial x} + \frac{g_a}{\omega_0} \frac{D_m}{a^4} \frac{\partial w}{\partial t} \right) \end{aligned} \tag{19}$$

where V_∞, M_∞ and ρ_a are the air flow speed, mach number and air density, respectively.

In addition, non-dimensional aerodynamic pressure is defined as

$$\lambda = \frac{\rho_a V_\infty^2 a^3}{\beta D_m} \tag{20}$$

while the non-dimensional aerodynamic damping parameter is given as

$$g_a = \frac{\rho_a V_\infty \left(M_\infty^2 - 2\right)}{\beta^3 \rho_m h \omega_0} \tag{21}$$

where,

$$\omega_0 = \sqrt{\frac{D_m}{\rho_m h a^4}} \tag{22}$$

is the convenient reference frequency.

$$\beta = \sqrt{M_\infty^2 - 1} \tag{23}$$

is the aerodynamic pressure parameter, respectively.

On the other hand, with using following approximation

$$\left(\frac{M_\infty^2 - 2}{M_\infty^2 - 1}\right)^2 \left(\frac{\mu}{\sqrt{M_\infty^2 - 1}}\right) \approx \frac{\mu}{M_\infty} \tag{24}$$

Which is valid for $M_\infty >> 1$, Eq. (21) can be approximated as [24]

$$g_a = \sqrt{\frac{\mu}{M_\infty} \lambda} \tag{25}$$

where μ is the air-mass ratio defined as $\mu = \rho_a a / \rho_m h$ [25].

Then the last term of Eq. (18) can be written by using the first-order piston theory as

$$\delta \boldsymbol{d}^T \boldsymbol{f} = \int_A p_a \delta w dA$$

$$= -\int_A \left(\lambda \frac{D_m}{a^3} \frac{\partial w}{\partial x} + \frac{g_a}{\partial \omega_0} \frac{D_m}{a^4} \frac{\partial w}{\partial t} \right) \delta w \, dA$$

$$= -\delta \boldsymbol{d}^T \left(\lambda \boldsymbol{A}_f \boldsymbol{d} + \frac{g_a}{\omega_0} \boldsymbol{A}_d \dot{\boldsymbol{d}} \right) \tag{26}$$

where $\boldsymbol{A}_f$ and $\boldsymbol{A}_d$ are the aerodynamic influence matrix and aerodynamic damping matrix, respectively.

The external virtual work in Eq. (15) can be represented as

$$\delta W_{ext} = -\delta \boldsymbol{d}^T \left(\boldsymbol{M} \ddot{\boldsymbol{d}} + \lambda \boldsymbol{A}_f \boldsymbol{d} + \frac{g_a}{\omega_0} \boldsymbol{A}_d \dot{\boldsymbol{d}} \right) \tag{27}$$

Substituting Eqs. (16) and (27) into Eq. (15), the equation of motion are obtained as

$$\boldsymbol{M} \ddot{\boldsymbol{d}} + \frac{g_a}{\omega_0} \boldsymbol{A}_d \dot{\boldsymbol{d}} + (\boldsymbol{K} - \boldsymbol{K}_{\Delta T} + \frac{1}{2} \boldsymbol{K} \boldsymbol{N}_1 + \frac{1}{3} \boldsymbol{K} \boldsymbol{N}_2 + \lambda \boldsymbol{A}_f) \boldsymbol{d} = \boldsymbol{P}_{\Delta T} \tag{28}$$

2.4 Solutions of Equation

2.4.1 *Linear equation*

To analyze linear vibration with thermal environment, the Eq. (28) is assumed to be

$$\boldsymbol{M}\ddot{\boldsymbol{d}} + (\boldsymbol{K} - \boldsymbol{K}_{\Delta T})\boldsymbol{d} = \boldsymbol{P}_{\Delta T} \tag{29}$$

In here, natural frequency is obtained using eigen value problem as

$$\boldsymbol{M}\ddot{\boldsymbol{d}} + \boldsymbol{K}_{L}\boldsymbol{d} = 0 \tag{30}$$

where $\boldsymbol{K}_{L} = \boldsymbol{K} - \boldsymbol{K}_{\Delta T}$.

To investigate the thermal buckling, the Eq.(29) is changed as

$$(\boldsymbol{K} - \boldsymbol{K}_{\Delta T})\boldsymbol{d} = 0 \tag{31}$$

2.4.2 *Post-buckling analysis*

In order to analyze post-buckling behavior, nonlinear equation is assumed as a sum of the static($\boldsymbol{d}_{s}$) and dynamic($\boldsymbol{d}_{t}$) part as $\boldsymbol{d} = \boldsymbol{d}_{s} + \boldsymbol{d}_{t}$. Subscript $\boldsymbol{s}$ and $\boldsymbol{t}$ denote the static and dynamic terms, respectively. In here, the static nonlinear equation is derived as

$$(\boldsymbol{K} - \boldsymbol{K}_{\Delta T} + \frac{1}{2}\boldsymbol{K}\boldsymbol{N}_{1} + \frac{1}{3}\boldsymbol{K}\boldsymbol{N}_{2} + \lambda \boldsymbol{A}_{f})\boldsymbol{d}_{s} = \boldsymbol{P}_{\Delta T} \tag{32}$$

Using the Newton-Raphson iterative method [26], the nonlinear behaviors of the model are obtained with function $\boldsymbol{\Psi}(\Delta \boldsymbol{d}_s)$ as

$$\boldsymbol{\Psi}(\Delta \boldsymbol{d}_s) = (\boldsymbol{K} - \boldsymbol{K}_{\Delta T} + \frac{1}{2}\boldsymbol{KN}_{1s} + \frac{1}{3}\boldsymbol{KN}_{2s} + \lambda\ \boldsymbol{A}_f)\Delta \boldsymbol{d}_s - \boldsymbol{P}_{\Delta T} \qquad (33)$$

To iterate the equation, the tangent stiffness $\boldsymbol{K}_{\tan_i}$ and load vector are derived as

$$\boldsymbol{K}_{\tan_i} = \left[\frac{d(\boldsymbol{\Psi}(\Delta \boldsymbol{d}_s))}{d(\Delta \boldsymbol{d}_s)}\right] = (\boldsymbol{K} - \boldsymbol{K}_{\Delta T} + \boldsymbol{KN}_{1s} + \boldsymbol{KN}_{2s} + \lambda\ \boldsymbol{A}_f)_i \qquad (34)$$

$$\boldsymbol{\Psi}(\Delta \boldsymbol{d}_s)_i = (\boldsymbol{K} - \boldsymbol{K}_{\Delta T} + \frac{1}{2}\boldsymbol{KN}_{1s} + \frac{1}{3}\boldsymbol{KN}_{2s} + \lambda\ \boldsymbol{A}_f)_i \Delta \boldsymbol{d}_{s_i} - \boldsymbol{P}_{\Delta T} \qquad (35)$$

The $i+1$ displacement vector can be calculated as

$$\boldsymbol{K}_{\tan_i} \Delta \boldsymbol{d}_{s_{i+1}} = -\boldsymbol{\Psi}(\Delta \boldsymbol{d}_s)_i \qquad (36)$$

$$\boldsymbol{d}_{s_{i+1}} = \boldsymbol{d}_{s_i} + \Delta \boldsymbol{d}_{s_{i+1}} \qquad (37)$$

And then, the post-buckling behaviors are iterated until the incremental displacement are converged.

2.4.3 *Limit cycle oscillation*

The time dependent part $\boldsymbol{d}_t$ is used to form the dynamic nonlinear equation as

$$\boldsymbol{M}\ddot{\boldsymbol{d}}_t + \frac{g_a}{\omega_0}\boldsymbol{A}_d\dot{\boldsymbol{d}}_t + (\boldsymbol{K} - \boldsymbol{K}_{\Delta T} + \boldsymbol{KN}_{1s} + \boldsymbol{KN}_{2s} + \lambda\boldsymbol{A}_f + \boldsymbol{KN}_{2st}\frac{1}{2}\boldsymbol{KN}_{1t} + \frac{1}{3}\boldsymbol{KN}_{2t})\boldsymbol{d}_t = \boldsymbol{P}_{\Delta T} \quad (38)$$

Eq.(38) is the equation of motion for vibration or flutter behaviors and is simplified like eigen-value problem as [27]

$$[\boldsymbol{K}_s + \lambda\boldsymbol{A}_s - k\boldsymbol{M}_s]\boldsymbol{\Phi} = 0 \quad (39)$$

where λ and k is non-dimensional aerodynamic pressure and eigenvalue, respectively. $\boldsymbol{\Phi}$ is generalized displacements vectors and assumed to be a harmonic motion as

$$\boldsymbol{\Phi} = \boldsymbol{\Phi}_0 e^{\omega t} \quad (40)$$

where $\boldsymbol{\Phi}_0$ is a time independent vector, and motion parameter $\omega = \omega_R + i\omega_I$ is a complex number. The aerodynamic matrix $\boldsymbol{A}_s$ is non-symmetric, and then the imaginary parts (ω_I) is expected for $\lambda > 0$. For $\lambda = 0$, the eigenvalues are real and positive because $\boldsymbol{K}_s$ and $\boldsymbol{M}_s$ are symmetric and positive definite. As λ is increased from zero, the eigenvalues become complex conjugate pairs when λ is λ_{cr}. Based on this method, the stability of the panel about flutter is calculated.

3. Numerical Results and Discussion

Vibration and buckling analysis of multifunctional antenna structure is performed and compared between the cases with heat conduction or without. The structure is composed by five layers, which are glass/epoxy(1mm), carbon/epoxy(1.2mm), a dielectric layer and honeycomb core(12.5mm), following Fig. 1. Also, the sequences of glass/epoxy and carbon/epoxy are $[\theta/\text{-}\theta]_s$ and $[0/\theta/90]_s$. The material properties are shown in Table. 1. The reference temperature is expressed as $T_{ref} = 300(\text{K})$ in this study. A 6x6 finite element mesh of 9-node in one element are used, and the phenol area is assumed to be a square having four elements in the plate. Additionally, the sets of boundary conditions are used

(a) Simply supported boundary conditions(S):

$v = w = \phi_y = 0$ at $x = 0, a$

$u = w = \phi_x = 0$ at $y = 0, b$

(b) Clamped boundary conditions(C):

$u = v = w = \phi_x = \phi_y = 0$ at $x = 0, a$ and $y = 0, b$

3.1 Thermoelastic linear analysis

In Fig. 2, the difference between heat conduction and uniform temperature case is compared. The temperature distribution of heat conduction is based on Eq.(1). On the other hand, uniform temperature is applied to the whole thickness direction with equal temperature. The reason to consider heat conduction is that the model is assumed to be under the supersonic

environment.

3.1.1 *Vibration behavior*

At first, a natural frequency of the model are investigated in thermal environment as solving the eigenvalue problem of Eq.(30). In here, a multifunctional structure is composed of composite layer. And then, code verification is performed with composite structure. Table. 2 shows a comparison of the fundamental natural frequencies of laminated composite plate with various thickness ratios for [0/90] layers. The non-dimensional parameter of the frequency $\Omega = \omega a^2 / (h\sqrt{E_2})$ presents sufficient accurate results as compared with previous data in Ref. [28,29]. In Fig. 3, the change of natural frequencies is presented with aspect ratio as temperature increases at the aspect ratio 60 and 40. The nondimension 1st natural frequencies are down to zero because the $\boldsymbol{K}_{\Delta T}$ of Eq.(29) is increased. And thus, the temperature at zero natural frequency means critical temperature of the model.

3.1.2 *Buckling behavior*

Another way to obtain the critical temperature is to solve the eigenvalue problem with Eq.(31). These results correspond with the data obtained from zero natural frequency. In order to verify the code of thermal buckling, critical temperatures of the sandwich composite structures are compared with previous results. The model's total thickness h consists of the two equal face sheets thickness h_f and core thickness h_c. The aspect a/b

and thickness ratio a/h is 1 and 20, respectively. And the layer sequence is $[0^\circ/90^\circ/.../0^\circ/90^\circ]^{10}$[core] $[90^\circ/0^\circ/.../90^\circ/0^\circ]^{10}$ with respect to the x-axis. The properties of structure as the face sheets and core are assumed to be constant irrespective of temperature changing. The result shows good agreement as in Table. 3 [30].

Table. 4 shows the critical temperature difference along aspect ratio with uniform and heat conduction conditions. The results of uniform case are lower than another case. The reason is that, in uniform case, all of layers is influenced as equal temperature, even though it is the lowest layer. And thus, following analyses are considered as heat conduction environment unless otherwise noted.

3.2 Aerothemoelastic nonlinear analysis

3.2.1 *Stability boundary*

Fig. 4 shows the stability region of the square isotropic plate with the nondimensional temperature (dT/dT_{cr}) and dynamic pressure (λ). The condition of region A is statically and dynamically stable. Region B is the buckled region where the panel is only statically unstable. Otherwise, Region C is flutter region that is dynamically unstable. Limit cycle oscillation is presented in this region. Generally, the results in this study have a good agreement with Ref. [31].

In Fig. 5, the stability region of the present model is shown with uniform and heat conduction cases. A region of heat conduction is decreased comparing with uniform case. In the other word, the flutter behavior of heat

conduction case is presented early on the same temperature.

3.2.2 *Postbuckling behavior*

The linear analysis of vibration and buckling are studied in the previous step, and the natural frequencies and critical temperatures are obtained in thermal conditions. From now on, post-buckling analyses are investigated from the Eq. (23). To obtain the verification of this study, the thermal post-buckling deflection of laminated composite plate is compared with the previous result of Averill and Reddy [32]. The layer thickness is 0.125mm, and thickness ratio is 150, and the sequence of the laminar is $[45/-45/0/90]_s$. Fig. 6 shows the center displacement of the plate as temperature rise. It has an good agreement with Ref. [32]. Two cases are applied to this study. One of the cases is uniform temperature rise, which means that the temperature is equal along the all layer. Another is that the temperature derived from heat conduction equation is applied to the model.

Fig. 7 (a) and (b) show deflection of the model as temperature rise by comparison of uniform case and heat conduction case. In Fig. 7 (a), the deflection at center of plate is increased as the non-dimensional temperature is increased for all cases. One of the different things between uniform and heat conduction cases is the time to start buckling. In uniform case, buckling is started more quickly than heat conduction case. The reason is that all of the layers are influenced from equal temperature. On the contrary, the bottom layer is relatively not effected by thermal condition. Fig. 7 (b) shows the deflection with temperature difference, not dimensional temperature. This figure also indicates that, in uniform case, the deflection is increased faster and the critical temperature is lower than another case. The tendency

influences the vibration behavior. In Fig. 8, even though the non-dimensional temperature is not enough to critical temperature, the fundamental natural frequency of uniform case is increased. On the other hand, the frequency of another case starts to increase at the critical temperature. As a result, the point between pre- and post-buckling is clearly able to make a division with heat conduction.

Fig. 9 (a) and (b) shows the deflection according to fiber angle. Because the model consists of various composite plates, the mechanical behavior is changed by fiber angle such as 90, 60 and 45. At first, the deflections of non-dimensional temperature case are similar with each other. However, the critical temperature at fiber angle 90 is lowest, and the case of fiber angle 30 is started buckling at the end in Fig. 9 (b). The vibration analysis of three case are performed in Fig. 9. At fiber angle 45, the deflection is a little big larger than other cases for pre- and post-buckling period.

One of the important things is the boundary conditions. All of the case in this paper is applied to simply supported conditions. However, in here, the differences between simply supported and clamped case are investigated in Fig. 10 (a) and (b). The deflection of the clamped case is almost clear to start at critical point. On the other hand, the deflection of simply supported case is already started to increase while the temperature approaches the critical temperature. Fig. 10 (b) also shows the same result that the natural frequency goes down to the zero value. When buckling starts, the one is increased again in simply-supported case.

3.2.3 *Limit cycle oscillation*

In this section, time analysis is performed with Newmark iteration method.

And thus, it is vital to set initial conditions. At first, the boundary condition is selected as simply supported and phenol area is 2×2 of 6×6 meshes except a special case. Additionally, ply angle of each layer is defined as 45°. The Aspect ratio and thickness ratio is $a/b=1$ and $a/h=100$, respectively. Based on the first-order piston theory, the deformation of the model is presented through x-direction. The air-mass ratio μ/M_{∞} is selected as 0.1. Finally, time step is 0.1ms.

In Fig. 11, the conditions for temperature difference (dT) and dynamic pressure (λ) are selected $4.38(K)$ and 1400, respectively. It means that this stability point is in C area in Fig. 6. The reason for selecting high dynamic pressure is that the limit cycle oscillation is presented early. The difference between uniform and heat conduction temperature conditions is shown in Fig. 11. In uniform temperature case, it reaches faster limit cycle than heat conduction case. The following results are applied as heat conduction condition. Fig. 12 (a) and (b) show the flutter behavior in the same temperature. Dynamic pressure (λ) is 1400, and other conditions are equal except temperature difference. At first, the behavior in Fig. 12 (a) is performed at the critical temperature, that is, the nondimensional temperature ($\Delta T/\Delta T_{cr}$) is 1. The temperature in Fig. 12 (b) is 10 times smaller than another case. As shown in those figures, the flutter behavior is started sooner than lower temperature conditions. Fig. 13 shows that the cycle is larger and faster than lower dynamic pressure. That is why the aerodynamic characteristics increase with the dynamic pressure. In Fig. 14, Flutter behaviors are shown with different dynamic pressures. The starting point of limit cycle oscillation is presented faster and bigger. Fig. 15 (a) and (b) shows how important the dynamic damping ratio which is assumed to be

0.1 without this case. Without the dynamic damping ratio, the limit cycle oscillation occurs with different frequencies not a dominant frequency.

4. Conclusions

The multifunctional antenna structure has many advantages such as reduction of drag, radar cross-section and weight. However, the structures is influenced by the aerodynamic and thermal loads, which may cause vibration and deformations of the model. Also, this aerothermoelastic characteristics will affect the degradation of the antenna performance. And then, numerous researches for the model have been performed in the field of the antenna performance.

In this work, the mechanical behaviors of the multifunctional antenna structure was investigated with heat conduction concepts. It contains linear analyses as well as nonlinear behavior in aerothermoelastic environment. To research large deformation, von-Karman strain-displacement relations was applied based on the first-order shear deformation plate theory. Also, the first-order piston theory was adopted for considering aerodynamic loads. The present model consists of different layers such as carbon/epoxy, glass/epoxy, a honeycomb core and a dielectric layer.

In the linear conditions, natural frequencies and critical temperatures are compared with uniform and distributed temperature boundary conditions. The natural frequencies in heat conduction are reduced to zero later than in uniform temperature condition. This results means that the buckling point of heat conduction case is presented later than another case. Thermal stability boundaries are also influenced by the concept. As considering the concept, the flutter area is broader. And thus, at the same temperature, the flutter behavior is started earlier than conventional case. Additionally, many parameter studied are focused on the influences of ply angle of face sheet,

aspect ratio and temperature difference.

In the future work, the antenna structure is required to consider the radiation patterns and performances of the model as well as the structure characteristics. And thus, the combination between two fields is vital. After this course, a vibration control is needed to improve antenna performance using a piezoeletric sensor and actuator.

References

[1] Tuss, J., Lockyer, A. J., Alt, K., Uldirich, F., Kinslow, R., Kudva, J. N., & Goetz, A. (1996). Conformal loadbearing antenna structure. In *37th AIAA struct dynamics mater conf, Salt Lake City, UT* (Vol. 836843).

[2] Callus, P. J. (2007). Conformal load-bearing antenna structure for Australian Defence Force aircraft.

[3] Varadan, V. K., & Varadan, V. V. (1994). Design and Development of Conformal Spiral Antenna with High Dielectric Materials and Chiral Absorbers. *JOURNAL OF WAVE MATERIAL INTERACTION*, *9*, 29-42.

[4] Lockyer, A. J., Alt, K. H., Coughlin, D. P., Durham, M. D., Kudva, J. N., Goetz, A. C., & Tuss, J. (1999, July). Design and development of a conformal load-bearing smart skin antenna: Overview of the AFRL smart skin structures technology demonstration (S3TD). In *1999 Symposium on Smart Structures and Materials* (pp. 410-424). International Society for Optics and Photonics.

[5] You, C. S., Hwang, W., & Eom, S. Y. (2005). Design and fabrication of composite smart structures for communication, using structural resonance of radiated field. *Smart Materials and Structures*, *14*(2), 441.

[6] Bishop, N. (2013). Ultrawideband (UWB) and Reconfigurable Antennas-New Concepts For Conformal Load Bearing Antenna Structures (CLAS).

[7] Knott, P., Loecker, C., Algermissen, S., & Sekora, R. (2012,

November). Compensation of static deformation and vibrations of antenna arrays. In *9TH INTERNATIONAL CONFERENCE ON MATHEMATICAL PROBLEMS IN ENGINEERING, AEROSPACE AND SCIENCES: ICNPAA 2012* (Vol. 1493, No. 1, pp. 573-578). AIP Publishing.

[8] Chaney, R. L., Hackler, D. R., Wilson, D. G., & Meek, B. N. Advanced Conformal Load-Bearing Antenna Structures.

[9] Loecker, C., Knott, P., Sekora, R., & Algermissen, S. (2012, March). Antenna design for a conformal antenna array demonstrator. In *2012 6th European Conference on Antennas and Propagation (EUCAP)* (pp. 151-153). IEEE.

[10] Pradeep, V., & Ganesan, N. (2008). Thermal buckling and vibration behavior of multi-layer rectangular viscoelastic sandwich plates. *Journal of Sound and Vibration*, *310*(1), 169-183.

[11] Matsunaga, H. (2007). Free vibration and stability of angle-ply laminated composite and sandwich plates under thermal loading. *Composite structures*, *77*(2), 249-262.

[12] Roh, J. H., Woo, J. H., & Lee, I. (2008). Thermal post-buckling and vibration analysis of composite conical shell structures using layerwise theory. *Journal of Thermal Stresses*, *32*(1-2), 41-64.

[13] Park, J. S., Kim, J. H., & Moon, S. H. (2005). Thermal post-buckling and flutter characteristics of composite plates embedded with shape memory alloy fibers. *Composites Part B: Engineering*, *36*(8), 627-636.

[14] Gibson, R. F. (2010). A review of recent research on mechanics of multifunctional composite materials and structures. *Composite*

structures, *92*(12), 2793-2810.

[15] Jeon, J. H., Hwang, W., Park, H. C., & Park, W. S. (2004). Buckling characteristics of smart skin structures. *Composite structures*, *63*(3), 427-437.

[16] Lee, C. Y., & Kim, J. H. (2014). Thermal Stability Characteristics and Limit Cycle Oscillation of Smart Skin Structures. *Journal of Thermal Stresses*, *37*(2), 221-235.

[17] Yoon, K. J., Kim, Y. S., Kim, Y. B., Lee, J. D., Park, H. C., Goo, N. S., & Lee, J. H. (2004). Parametric study on compression deformation behavior of conformal load-bearing smart skin antenna structure. In *Key Engineering Materials* (Vol. 261, pp. 663-668). Trans Tech Publications.

[18] Park, J. S., & Kim, J. H. (2006). Thermal postbuckling and vibration analyses of functionally graded plates. *Journal of Sound and Vibration*, *289*(1), 77-93.

[19] Kulkarni, M. R., & Brady, R. P. (1997). A model of global thermal conductivity in laminated carbon/carbon composites. *Composites science and Technology*, *57*(3), 277-285.

[20] Venart, J. E. S., & Prasad, R. C. (1980). Thermal conductivity of phenol (C6H5OH). *Journal of Chemical and Engineering Data*, *25*(3), 198-199.

[21] Vlachoutsis, S. (1992). Shear correction factors for plates and shells. *International Journal for Numerical Methods in Engineering*, *33*(7), 1537-1552.

[22] Reddy, J. N. (2004). *Mechanics of laminated composite plates and shells: theory and analysis*. CRC press.

[23] Dixon, S. C. (1966). Comparison of panel flutter results from approximate aerodynamic theory with results from exact inviscid theory and experiment.

[24] Liao, C. L., & Sun, Y. W. (1993). Flutter analysis of stiffened laminated composite plates and shells in supersonic flow. *AIAA journal*, *31*(10), 1897-1905.

[25] Prakash, T., & Ganapathi, M. (2006). Supersonic flutter characteristics of functionally graded flat panels including thermal effects. *Composite Structures*, *72*(1), 10-18.

[26] Cook, R. D. (2007). *Concepts and applications of finite element analysis*. John Wiley & Sons.

[27] OLSON, M. D. (1970). Some flutter solutions using finite elements. *AIAA Journal*, *8*(4), 747-752.

[28] Akoussan, K., Boudaoud, H., Daya, E. M., & Carrera, E. (2015). Vibration modeling of multilayer composite structures with viscoelastic layers. *Mechanics of Advanced Materials and Structures*, *22*(1-2), 136-149.

[29] Matsunaga, H. (2007). Free vibration and stability of angle-ply laminated composite and sandwich plates under thermal loading. *Composite structures*, *77*(2), 249-262.

[30] Matsunaga, H. (2005). Thermal buckling of cross-ply laminated composite and sandwich plates according to a global higher-order deformation theory. *Composite Structures*, *68*(4), 439-454.

[31] Xue, D. Y., & Mei, C. (1993). Finite element nonlinear panel flutter with arbitrary temperatures in supersonic flow. *AIAA journal*, *31*(1), 154-162.

[32] Averill, R. C., & Reddy, J. N. (1993, January). Thermomechanical postbuckling analysis of laminated composite shells. In *The 34th AIAA/ASME/ASCE/AHS/ASC Structures, Structural Dynamics and Materials Conference, AIAA-93-1337-CP* (pp. 351-60).

Table 1. Material properties of the smart skin[17,19,20]

	G/E	C/E	Phenol	Honeycomb
E_1	24Gpa	67Gpa	7.2Gpa	0.09Mpa
E_2	28Gpa	57Gpa		0.08Mpa
ν_{12}	0.105	0.103	0.3	0.3
G_{12}	4.54Gpa	5.9Gpa		0.1Mpa
G_{13}	1.0Gpa	1.0Gpa		19.7Mpa
G_{23}	1.0Gpa	1.0Gpa		11.5Mpa
α_1	9.7^{-6}/℃	2.1^{-6}/℃		1.5^{-6}/℃
α_2	17.7^{-6}/℃	2.1^{-6}/℃		1.5^{-6}/℃
ρ	2200kg/m^3	1450kg/m^3	9000kg/m^3	96.1kg/m^3
k	0.686W/mK	1.5 W/mK		170 W/mK

Table. 2 Natural frequency of the composite plates with thickness ratio for $[0^{\circ}/90^{\circ}]_s$.

Cases	*a/h*			
Results	10	20	50	100
Present	15.057	17.580	18.600	18.764
Ref.[28]	15.150	17.626	18.599	18.805
Ref.[29]	15.153	17.628	18.600	18.804

Table. 3 Critical temperatures of the sandwich plates with h_f / h

Cases	h_f / h		
	0.05	0.1	0.15
Present	0.09522	0.08692	0.07976
Ref.[30]	0.09498	0.08667	0.07954

Table. 4 Critical temperature vs aspect ratio with different heat environment

Cases	*a/h*			
Results	40	60	80	100
Uniform	130	60.13	34.24	22.04
Heat Conduction	260	119	68.30	43.96

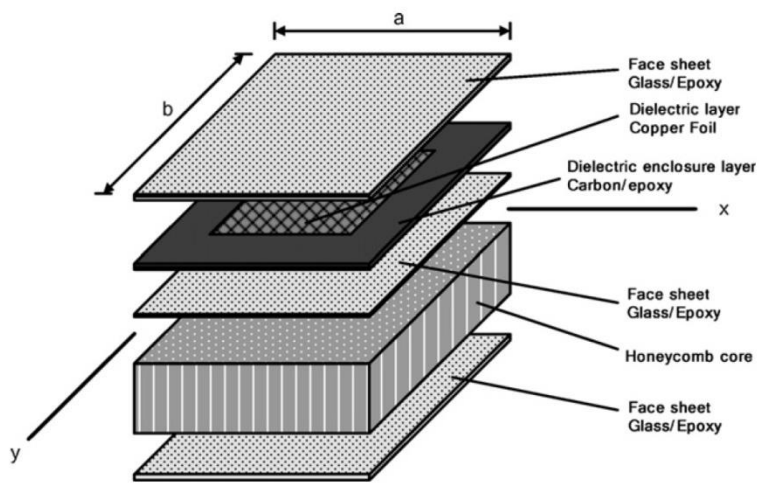

Fig. 1 Simplified model of a multifunctional antenna structure

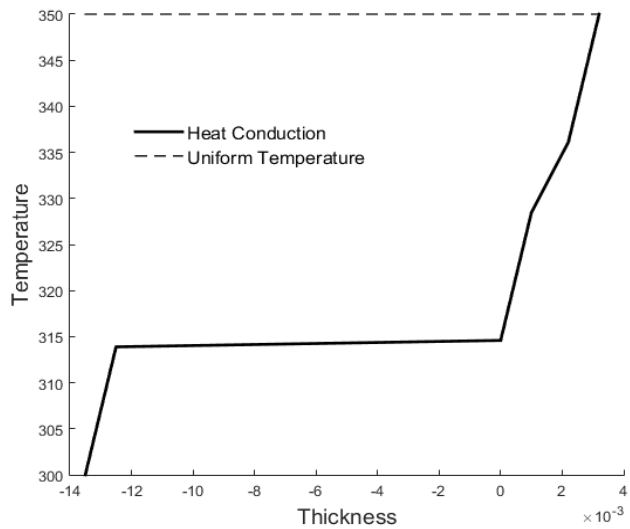

Fig. 2 The temperature difference with uniform case and heat conduction

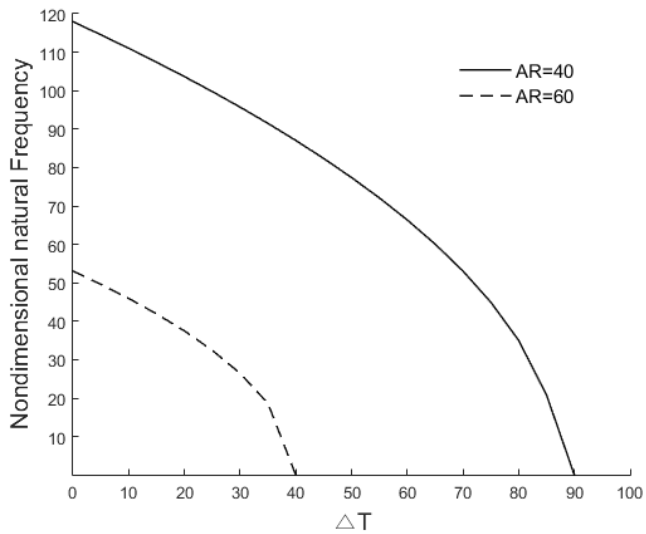

Fig. 3 Nondimensional natural frequency with temperature

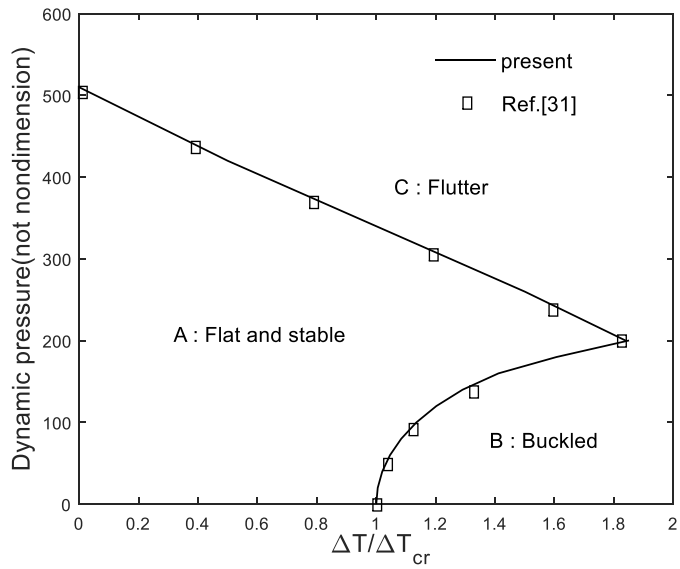

Fig. 4 Thermal stability boundaries of isotropic panel

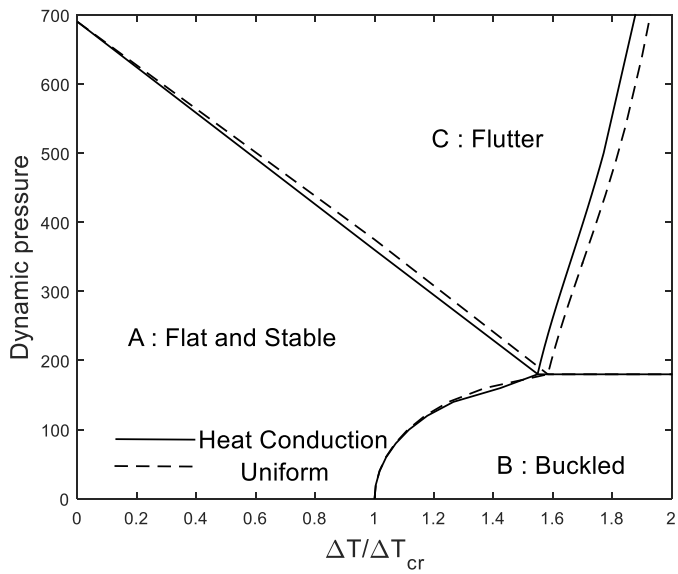

Fig. 5 Thermal stability boundaries of the present model

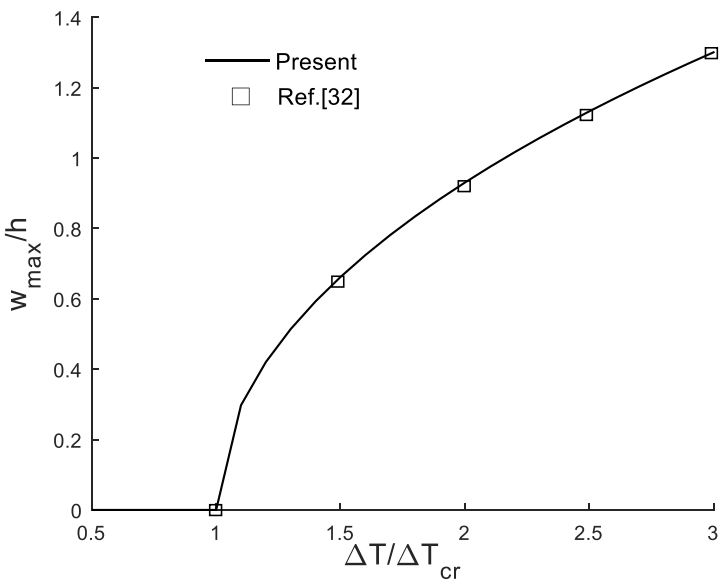

Fig. 6 Center deformation of the model with uniform temperature difference

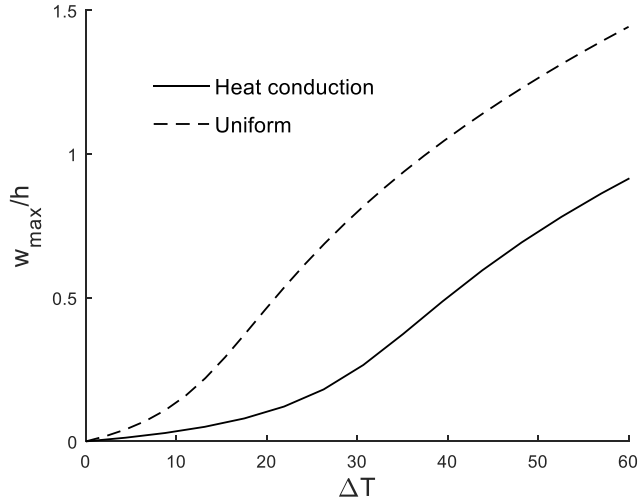

(a) with a nondimensional temperature

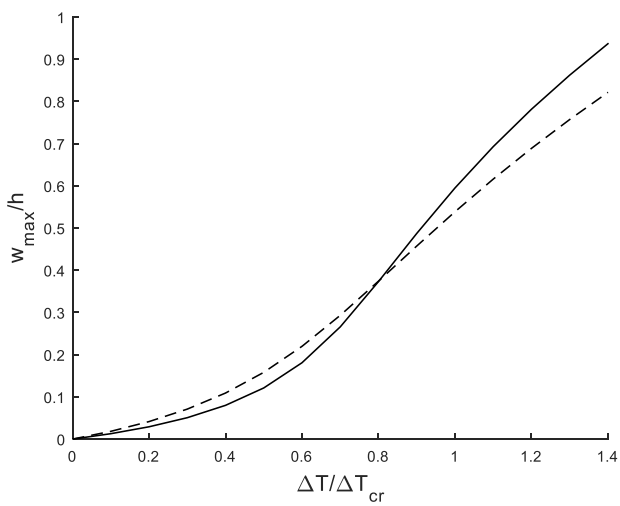

(b) with a temperature

Fig. 7 Deflection with heat conduction

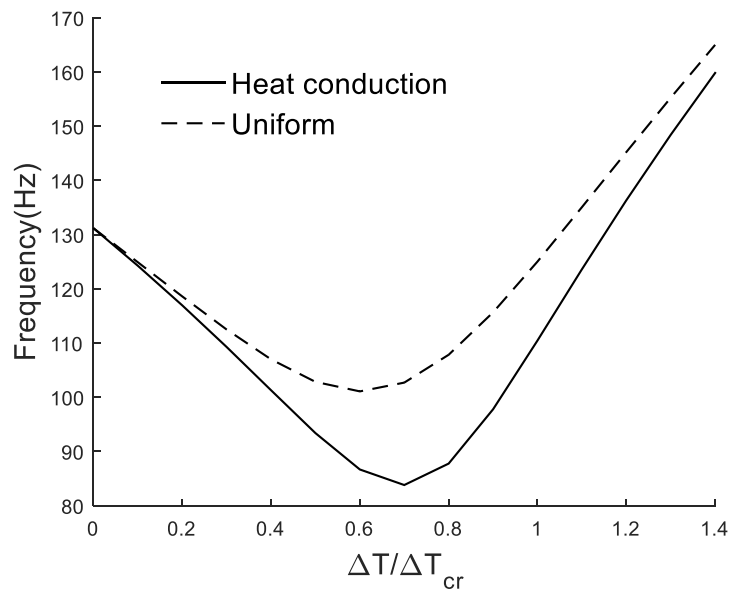

Fig. 8 Fundamental natural frequency with heat conduction

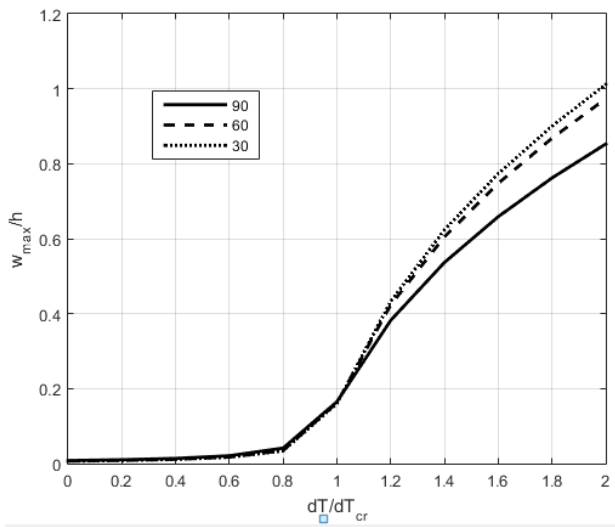

(a) with a nondimensional temperature

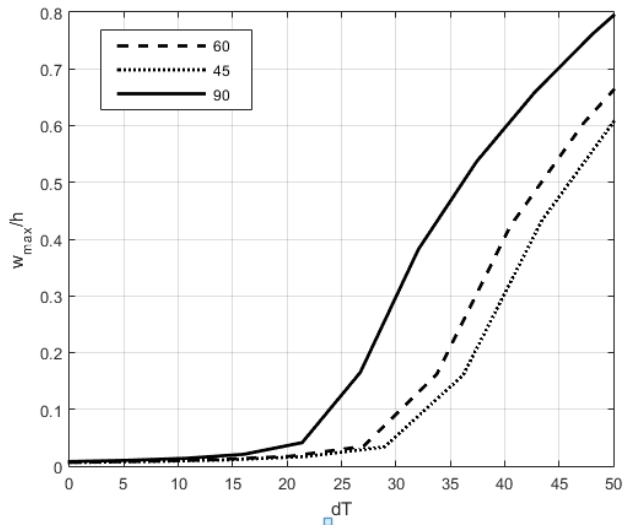

(b) with temperature difference

Fig. 7 Deflection with fiber angle

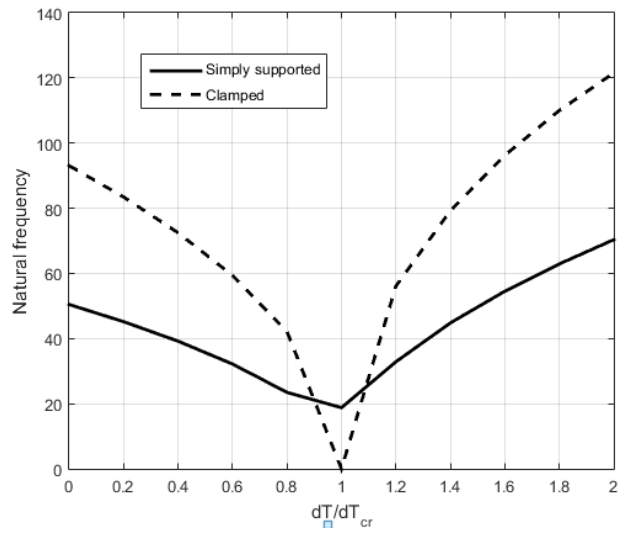

(a) Natural frequency

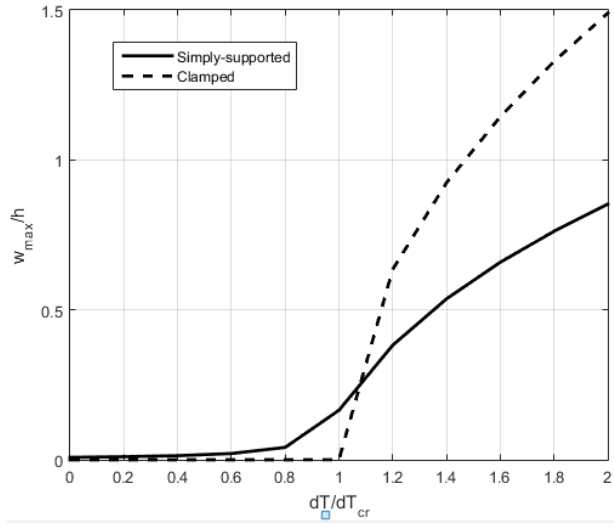

(b) Deflection

Fig. 10 Comparison with clamped and simply-supported

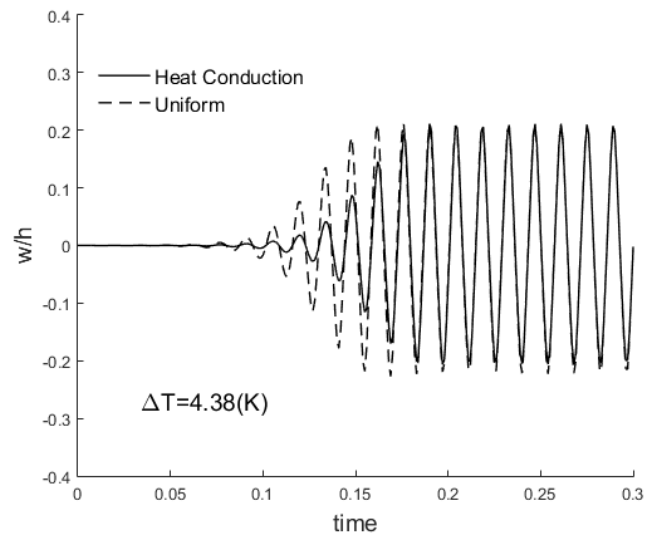

Fig. 11 Flutter behavior with uniform vs heat conduction

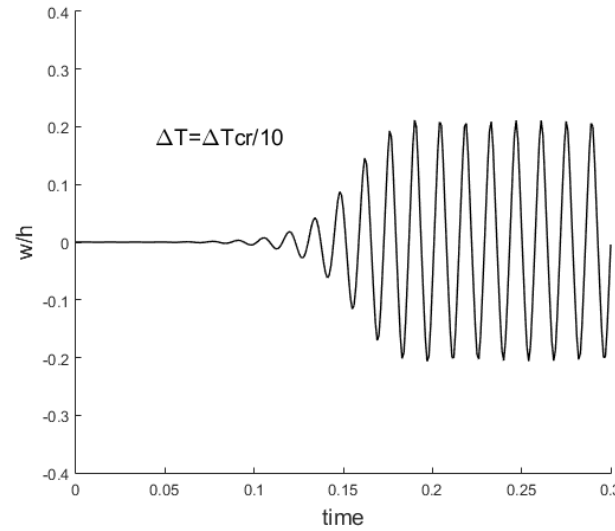

(a) $\Delta T = \Delta Tcr$

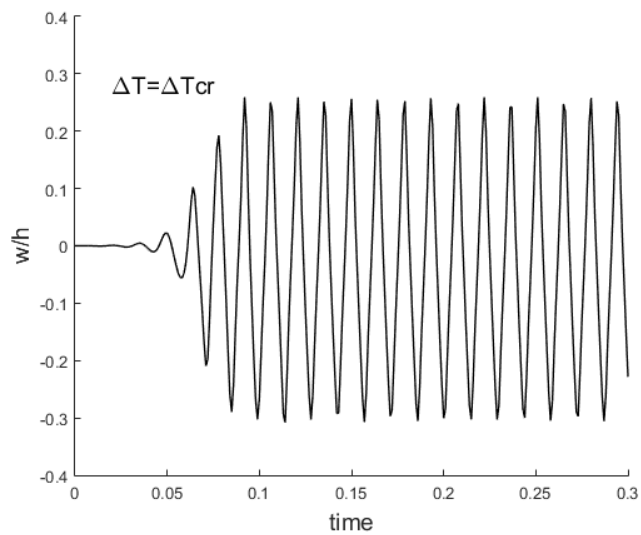

(b) $\Delta T = \Delta Tcr/10$

Fig. 12 Flutter behavior with different temperature conditions

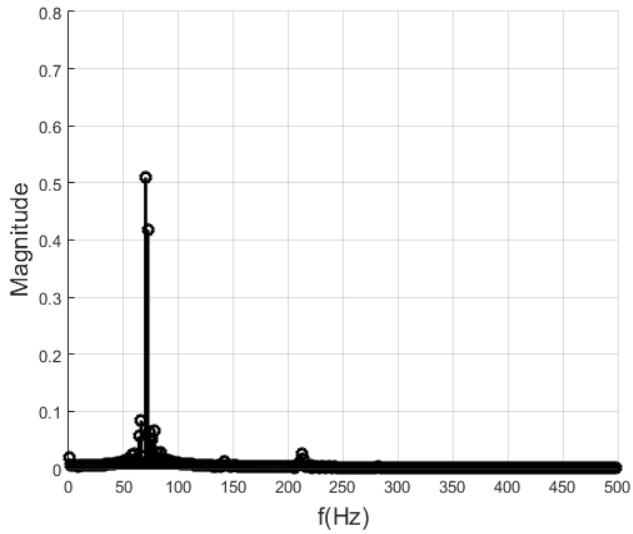

(a) $\Delta T = \Delta Tcr$

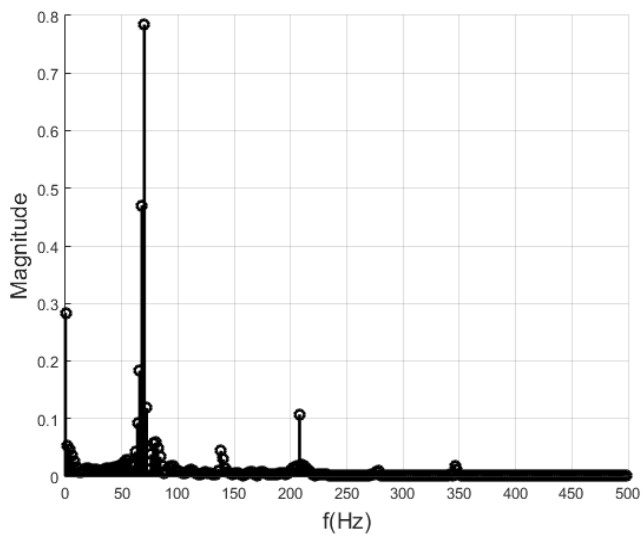

(b) $\Delta T = \Delta Tcr/10$

Fig. 13 Frequency spectrum with different temperature conditions

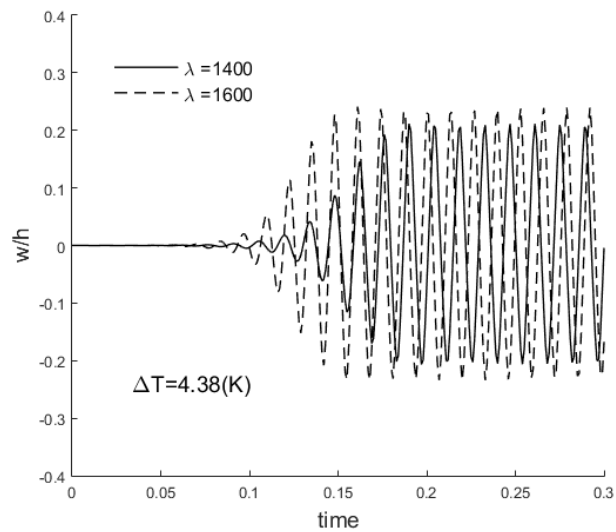

Fig. 14 Flutter behavior with different dynamic pressures

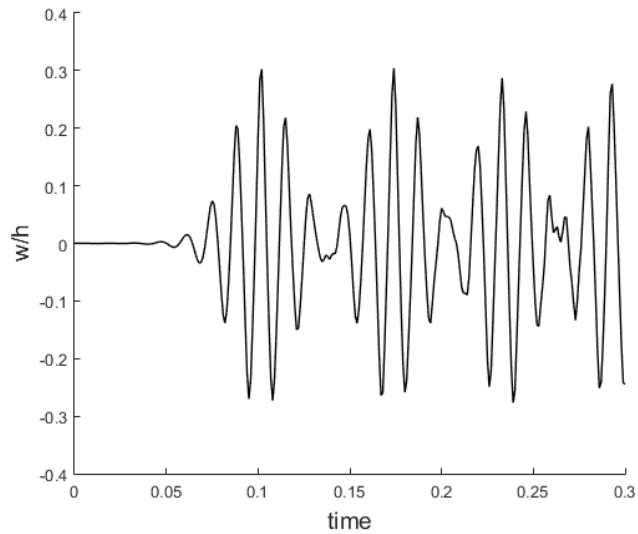

(a) Time spectrum

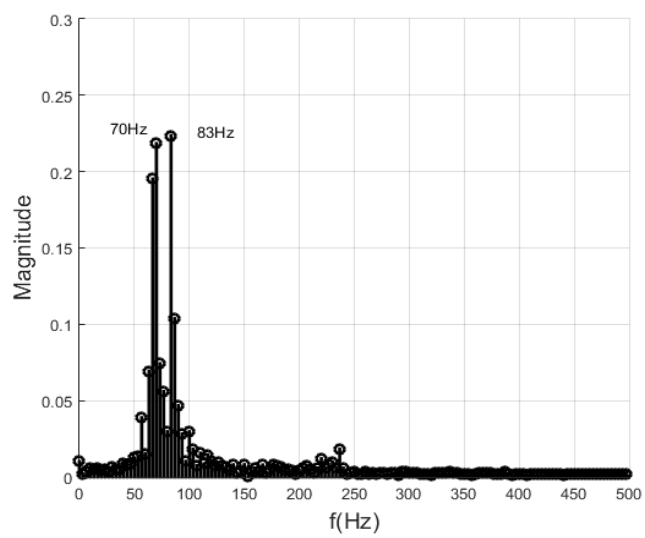

(b) Frequency spectrum

Fig. 15 Time and frequency spectrum without dynamic damping ratio

국 문 초 록

안테나가 내장되어 있는 다기능 안테나 구조물의 진동 및 좌굴 현상에 대한 연구를 진행하였다. 본 연구에 사용된 구조물은 다중 샌드위치 구조물로써 carbon/epoxy, glass/epoxy, 유전체로 구성되었으며, 1차 전단 변형 판 이론을 사용하여 모델링을 하였다. 또한 변형의 기하학적인 비선형성을 고려하기 위하여 von-Karman 변형-변위 관계식을 적용하여 지배방정식을 이끌어냈다. 초음속으로 가정된 상황을 고려하여 1차 피스톤 이론을 통해 공기력이 적용되었으며 열적 경계 조건으로는 1차 열전도 관계식이 사용하였다. 수치적 결과는 유한요소법을 기본으로 하며, 비선형 해석을 위해 Newton-Rhapson 반복계산법과 시간 해석을 위한 Newmark 수치해석법이 사용되었다. 수치적 결과의 신뢰성을 판단하기 위해, 기존의 행해졌던 연구와의 데이터 비교가 진행되었다.

본 연구에서는 단일 온도 효과를 적용했을 경우와 1차 열전도 관계식을 도입했을 경우를 비교 및 분석하여 실제 항공기의 운용 조건을 현실적으로 고려하고자 했다. 이를 통해, 고유진동수, 임계 온도 및 제한주기운동의 물리적 거동에 미치는 영향을 분석하였다.

Keywords: 다기능 내장 안테나 구조물, 좌굴, 진동, 제한주기운동, 열전도.

Student Number: 2015-20763